Journal of Vision (2010) 10(3):18, 1–19 http://journalofvision.org/10/3/18/

Curvature coding is tuned for motion direction

Elena Gheorghiu Laboratory of Experimental Psychology, University of Leuven, Leuven, Belgium

Frederick Kingdom McGill Vision Research, Department of Ophthalmology, McGill University, Montreal, Quebec, Canada

Rickul Varshney McGill Vision Research, Department of Ophthalmology, McGill University, Montreal, Quebec, Canada

We have investigated the global and local motion tuning properties of curvature coding mechanisms using two shape after-effects believed to be mediated by curvature-sensitive mechanisms: the shape-frequency after-effect, or SFAE, and the shape-amplitude after-effect, or SAAE. The SFAE and SAAE are the phenomena in which adaptation to a sine-wave-shaped contour causes a shift in respectively the apparent shape-frequency and apparent shape-amplitude of a test contour in a direction away from that of the adapting stimulus. In the global motion condition the sinusoidal-shaped contours were made to drift within a fixed stimulus window in the direction of their axis of modulation. In the local motion condition the contour was constructed from a string of Gabors, and their carriers but not envelopes moved. We investigated selectivity to motion direction by using adaptor and test contours that moved either in the same or opposite directions. We found that in the global motion condition both the SFAE and SAAE showed selectivity to motion direction, and that for the same-motion-direction condition, both after-effects increased with shape temporal frequency. We then examined the effect of luminance spatial frequency and luminance temporal frequency on global motion direction selectivity. Luminance temporal frequency accounted for some of the increase in after-effect magnitude with shape temporal frequency, but shape temporal frequency also contributed. The local motion after-effects on the other hand were neither selective to motion direction nor increased with luminance temporal frequency. Taken together, the results are best understood by supposing that curvature is encoded by mechanisms that are selective to motion direction and that the directional selectivity best manifests itself psychophysically when there is sufficient spatio-temporal coverage of the stimulus to stimulate the full array of potentially responsive curvature-coding mechanisms.

Keywords: motion, temporal-frequency, shape, curvature, adaptation, after-effect

Citation: Gheorghiu, E., Kingdom, F., & Varshney, R. (2010). Curvature coding is tuned for motion direction. *Journal of Vision, 10*(3):18, 1–19, http://journalofvision.org/10/3/18/, doi:10.1167/10.3.18.

Introduction

It is widely believed that in primates shape processing is mediated primarily by the ventral pathway and global motion processing primarily by the dorsal pathway (Baizer, Ungerleider, & Desimone, 1991; Maunsell & van Essen, 1983; Merigan & Maunsell, 1993; Shipp, 1995). There is good evidence however that shape and motion processing interact. For example, neurophysiological studies have shown that neurons in ventral areas V4 and IT are sensitive to shapes defined solely by coherent motion of random dots (Mysore, Vogels, Raiguel, & Orban, 2006, 2008; Sary, Vogels, Kovacs, & Orban, 1995; Sary, Vogels, & Orban, 1993; Wang et al., 1999). Moreover, anatomical studies have revealed strong connectivities between the motion-sensitive dorsal area MT and the contour-shape-sensitive ventral area V4 (Maunsell & van Essen, 1983; Merigan & Maunsell, 1993; Ungerleider & Desimone, 1986; Van Essen, Maunsell, & Bixby, 1981).

In this communication we ask whether mechanisms that encode curvature are selective to motion direction. The question is pertinent because different considerations concerning the relationship between motion and curvature lead to different expected outcomes. One outcome is predicated on the idea that shape-processing is not only a multi-stage process following a hierarchy from simple to complex shapes (Connor, Brincat, & Pasupathy, 2007; Gallant, Braun, & Van Essen, 1993; Gallant, Connor, Rakshit, Lewis, & Van Essen, 1996; Habak, Wilkinson, Zakher, & Wilson, 2004; Levi & Klein, 2000; Missal, Vogels, Li, & Orban, 1999; Murray, Kersten, Olshausen, Schrater, & Woods, 2002; Pasupathy & Connor, 2001, 2002; Regan & Hamstra, 1992; Tanaka, 1996; Wilkinson, Wilson, & Habak, 1998), but that as one proceeds though the shape-processing hierarchy, information about non-shape stimulus attributes such as luminance contrast, color contrast, contrast polarity, luminance spatial frequency, motion direction and depth is gradually discarded in order to make the higher stages of shape processing invariant to these attributes (Anderson, Habak, Wilkinson, & Wilson,

doi: 10.1167/10.3.18 Received August 3, 2009; published March 30, 2010 ISSN 1534-7362 © ARVO

2007; Bell & Kingdom, 2009; Gheorghiu, Kingdom, Thai, & Sampasivam, 2009; Ito, Tamura, Fujita, & Tanaka, 1995; Mysore et al., 2006). For example curvature processing is not tuned to stereoscopic depth, suggesting that stereoscopic depth is discarded by the middle stages of the shape-processing hierarchy (Gheorghiu et al., 2009). On these grounds therefore we might expect curvature processing to be *non-selective* to motion direction.

On the other hand several psychophysical studies have revealed motion direction selectivity for various spatial after-effects such as the tilt after-effect (Apthorp & Alais, 2009; Carney, 1982a, 1982b) and size after-effect (Nishida, Motoyoshi, & Takeuchi, 1999), suggesting that motion direction tuning is preserved throughout the shape-processing hierarchy. Motion direction selectivity has also been reported for the speed aftereffect (Thompson, 1981).

What have studies specifically examining interactions between motion and contour shape revealed? A few studies have examined the effect of motion on contour detection and global shape discrimination, using contours made of strings of Gabor elements in which the carriers move inside stationary envelopes. This type of motion is here termed 'local' motion, as opposed to when the entire Gabor or contour moves which is termed here 'global' motion. Contours made from Gabor strings that are surrounded by 'noise' Gabors are more easily detected when their local motions are such as to bring the Gabor elements into apparent spatial alignment (Hayes, 2000), and spatially aligned Gabor-string contours are more easily detected when their local motions are coherent rather than not (Bex, Simmers, & Dakin, 2003; Hess & Ledgeway, 2003; Ledgeway & Hess, 2002). However the contour-detection studies, while demonstrating that motion is a powerful cue for helping to detect a contour in noise, are not necessarily germane to curvature coding. Arguably of more direct relevance are those studies that have measured the detection of purely local-motion-defined radial-frequency (or RF) patterns (Rainville & Wilson, 2004, 2005). In this paradigm, the purely local motions of circular arrangements of Gabors elicit compelling impressions of a global RF pattern. Rainville and Wilson (2004, 2005) have argued that local-motion-induced RF shapes are not merely generated from local shifts in the positions of the Gabors caused by their carrier motions (e.g. as demonstrated by De Valois & De Valois, 1991), but are instead generated by a motion-integration mechanism specialized for delivering global shapes, albeit one that interacts with global shapes generated from static pattern information. However, although studies of motion-induced RF patterns reveal that local motion signals can be used to encode global shape, they do not test whether those shapes are *labeled* for the direction of the local motions that induces them.

A single study by Loffler and Wilson (2001) investigated the interaction between *global* motion and contour shape. Loffler and Wilson measured thresholds for detecting an RF pattern composed of two rotating RF components (RF2 + RF3), producing RF patterns that appeared to rotate, either rigidly or non-rigidly. Thresholds were measured in the presence of moving vertical and radial grating masks, and concentric gratings masks that moved orthogonally to the RF contour. Loffler and Wilson found that thresholds were least elevated for mask gratings with horizontal translational motion and most elevated for rotating and expanding/contracting masks. They concluded that the motion inputs to global shape were not simple local motions but complex patterns of global motion. However once again, while the Loffler and Wilson study has helped to establish the nature of the motion inputs to global shape processing, it leaves open the question as to whether shapes, once encoded, are labeled for their direction of motion. To our knowledge no study has thus investigated whether curvature and other shape mechanisms are *tuned* to either global and/or local motion direction, nor whether these mechanisms are sensitive to temporal frequency.

In addition, no studies have to our knowledge investigated how the luminance-contrast properties of contour-shapes, such as luminance scale or spatial frequency, might influence how contour shape and motion direction interact. Several studies have shown that luminance scale is an important factor for static contour-shape perception (Gheorghiu & Kingdom, 2006; Wilson & Richards, 1989). For example with static shapes two of us have found that contour-shape mechanisms show a degree of selectivity to luminance scale (Gheorghiu & Kingdom, 2006). Wilson and Richards (1989) have shown that curvature discrimination thresholds for contours are unimpaired by high-pass but impaired by low-pass luminance filtering, while Prins, Kingdom, and Hayes (2007) found that the detection of the low shape-frequency component of a jagged, or fractal edge, was not significantly impaired by either high-pass or low-pass filtering. These last two studies agree that fine luminance scales can mediate the efficient coding of contour shape but disagree as to whether coarse luminance scales are also involved. The effect of luminance scale on the interaction between global motion and contour shape has yet however to be determined.

We have employed two shape after-effects to study the motion direction tuning of curvature processing: the shape-frequency after-effect, or SFAE, and the shape-amplitude after-effect, or SAAE. These are the perceived shifts in respectively the shape-frequency and shape-amplitude of a sinusoidal test contour following adaptation to a sinusoidal contour of slightly different shape-frequency/shape-amplitude. In previous studies, we have shown that the SFAEs/SAAEs are mediated by mechanisms that encode curvature, rather than local orientation, periodicity, luminance spatial-frequency, position or global shape (Gheorghiu & Kingdom, 2007a, 2007b, 2008, 2009).

In order to determine whether the SFAE and SAAE are selective to motion direction we compared the after-effects for adaptor/test contours moving in the same versus opposite directions. If the after-effects are significantly larger for the same-direction condition this suggests that curvature-encoding mechanisms are selective for motion direction.

General methods

Observers

Eight subjects participated in different experiments. Three subjects were the authors (EG, FK, RV) and five subjects (JB, MS, NN, KV, SM) were naive with regard to the experimental aims. All subjects had normal or corrected-to-normal visual acuity. Each subject gave informed consent prior to participation in accordance with the university guidelines.

Stimuli

The stimuli were generated by a ViSaGe video-graphics card (Cambridge Research Systems) with 12-bits contrast resolution, presented on a calibrated, gamma-corrected Sony Trinitron monitor, running at 120 Hz frame rate and with a spatial resolution of 1024 × 768 pixels. The mean luminance of the monitor was 42 cd/m^2. Viewing distance was 100 cm.

Adaptation and test stimuli consisted of pairs of sine-wave-shaped contours. Each pair of adapting and test contours consisted of one contour moving to the left and another moving to the right. Example stimuli are shown in Figure 1 and a movie in Appendix A. Unless otherwise stated, the adaptor pair for the SFAE consisted of contours with a shape-amplitude of 0.43 deg and shape frequencies of 0.25 and 0.75 c/deg, giving a geometric mean shape-frequency of 0.43 c/deg. For the SAAE, the shape-frequency of the adaptor pair was 0.43 c/deg, while the shape-amplitudes were 0.25 and 0.75 deg, giving a geometric mean shape-amplitude of 0.43 deg.

The two adaptor and test contours were presented at 3.5 deg above and below the fixation marker. The cross-sectional luminance profile of the contours was odd-symmetric and was generated according to a first derivative of a Gaussian function:

$$L(d) = L_b \pm L_b \cdot C \cdot \exp(0.5) \cdot (d/\sigma) \cdot \exp\left[-(d^2/(2\sigma^2))\right], \tag{1}$$

where d is the distance from the midpoint of the contour's luminance profile along a line perpendicular to the tangent, L_b is background luminance of 42 cd/m^2, C contrast and σ the space-constant. Unless otherwise stated, the contrast C was set to 0.5 and σ to 0.044 deg. The ± sign determined the polarity of the contour. Our contours were designed to have a constant cross-sectional width, and the method used to achieve this is given in Gheorghiu and Kingdom (2006).

Procedure

Each session began with an initial adaptation period of 90 s, followed by a repeated test of 1 s duration interspersed with top-up adaptation periods of 3 s. For the static condition only, during the adaptation and test periods the shape-phase of the contour was randomly changed every 1 s in order to prevent the formation of afterimages and to minimize the effects of local orientation adaptation. The presentation of the test contour was signaled by a tone. Subjects were required to fixate on the marker placed between each pair of contours for the entire session. A head and chin rest helped to minimize head movements.

A staircase method was used to estimate the point of subjective equality (or PSE). For the SFAE the geometric mean shape-frequency of the two test contours was held constant at 0.43 c/deg while the computer varied the relative shape-frequencies of the two tests in accordance with the subject's response. At the start of the test period the ratio of the two test shape-frequencies was set to a random number between 0.71 and 1.4. On each trial subjects indicated via a button press whether the upper or lower test contour had the higher perceived shape-frequency. The computer then changed the ratio of test shape-frequencies by a factor of 1.06 for the first five trials and 1.015 thereafter, in a direction opposite to that of the response, i.e. towards the PSE. The session was terminated after 25 trials. In order that the total amount of adaptation for each condition was the same, we used a staircase method that was terminated after a fixed number (25) of trials, rather than a fixed number of reversals. We found in pilot studies that 25 trials were generally sufficient to produce a convergence that was stable over the last 20 trials. The shape-frequency ratio at the PSE was calculated as the geometric mean shape-frequency ratio of the two tests averaged across the last 20 trials, with the ratio's nominator the test that followed the lower shape-frequency adaptor and its denominator the test that followed the higher shape-frequency adaptor. For each *with-adaptor* condition we made six measurements, three in which the upper adaptor had the higher shape-frequency and three in which the lower adaptor had the higher shape-frequency. In addition we measured for each condition the shape-frequency ratio at the PSE in the absence of the adapting stimulus (the *no-adaptor condition*). To obtain an estimate of the size of the SFAE we first calculated the difference between the logarithm of each with-adaptor shape-frequency ratio at the PSE and the mean of the logarithms of the no-adaptor shape-frequency ratios at the PSE. We then calculated the mean

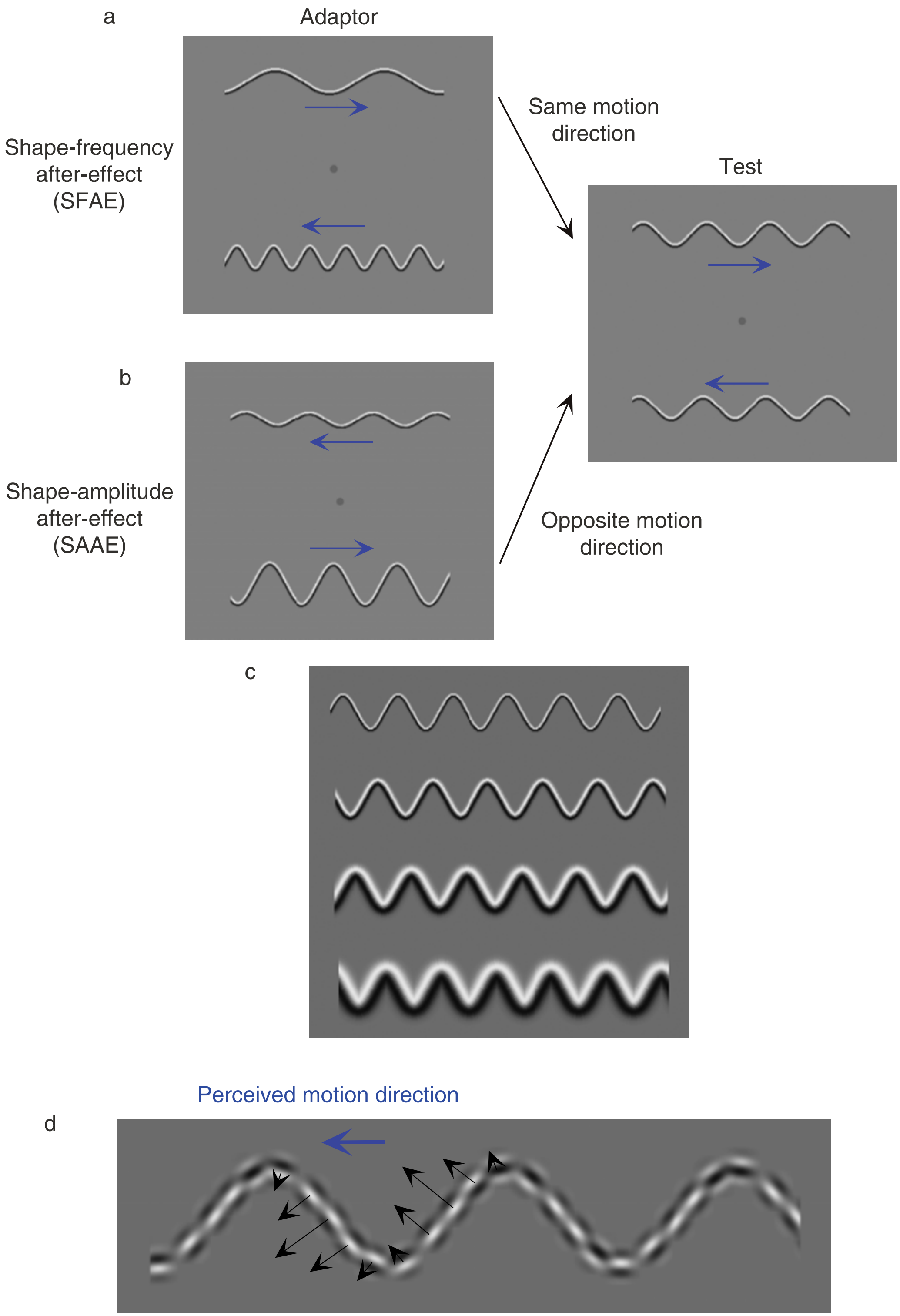

Figure 1. Stimuli used in the experiments. One can experience (a) the shape-frequency after-effect (SFAE) and (b) the shape-amplitude after-effect (SAAE) with a static contour by fixating the markers located midway between the pair of adapting contours (left) for about a minute, and then shifting one's gaze to the middle of the two identical test contours (right). In the experiments each pair of adapting and test contours consists of one contour moving to the left and the other moving to the right. (c) Example contours used in Experiments 2 and 3. The contours were constructed with odd-symmetric luminance profiles of various space-constants σ. There were four σs: 0.122, 0.088, 0.044 and 0.022 deg. (d) Example contours used in Experiment 4. The contours were constructed from Gabors with stationary envelopes and moving carriers. The orientation of each Gabor was tangential to the curve of the shape waveform. Black arrows indicate the carrier directions and relative temporal frequencies of each Gabor, simulating rigid-body motion as indicated by the blue arrow (see text for details).

and standard error of these differences across the six measurements, and these are the values shown in the graphs.

The procedure for measuring the SAAE followed the same principle as for the SFAE. The computer varied the relative shape-amplitudes of the two tests in accordance with the subject's response, while the geometric mean shape-amplitude of the two test contours was held constant at 0.43 deg.

Experiments and results

Experiment 1: Global motion-direction tuning

In this experiment we examine the global motion-direction selectivity of the SFAE and SAAE as a function of shape temporal frequency. If curvature-coding mechanisms are selective for global motion-direction, we expect that the after-effects will be reduced when the adaptor and test contours move in opposite compared to the same direction.

Adaptation and test stimuli consisted of pairs of moving sine-wave-shaped contours. A pair consisted of a contour positioned above and a contour positioned below fixation, moving in opposite directions. There were two arrangements: (i) contour above fixation moving to the left and contour below fixation moving to the right, and (ii) vice-versa. There were two adaptor-test conditions for each of these two arrangements: (i) adaptor and test moving in the *same* direction, and (ii) adaptor and test moving in *opposite* directions. Example stimuli are shown in Figures 1a and 1b and a movie in Appendix A. We varied the temporal frequency of the continuously moving adaptor and test contours. We used five shape temporal frequencies: 1, 1.57, 2.45, 3.83 and 6 cycles/sec. Note that although a temporal cycle here refers to a cycle of shape modulation, it also refers to a cycle of luminance modulation, as the cross-sectional luminance profile of the contour is a single biphasic function. In addition, we measured after-effects for static adaptor and test contours whose shape-phase changed randomly every 0.5 sec (the static condition).

Figure 2 shows the SFAEs (Figure 2a) and SAAEs (Figure 2b) as a function of shape temporal frequency for the same (open symbols) and opposite (filled symbols) adaptor-test motion direction conditions. The dashed lines indicate the size of after-effects obtained with static adaptors and test contours whose shape-phase changed randomly every 0.5 sec.

The results show that SFAEs and SAAEs (i) are significantly reduced when the adaptor and test contours move in opposite directions, (ii) increase in magnitude with shape temporal frequency, provided the adaptor and test have the same motion direction, and (iii) remain approximately constant across shape temporal frequency when adaptor and test have opposite motion directions. These results indicate that SFAEs and SAAEs are selective to global motion direction.

We ran a one-factor within-subjects ANOVA for the factor Motion direction (same vs. opposite) and found a significant difference between the same and opposite conditions for both the SFAE ($F(1,28) = 23.68$, $p < 0.05$) and SAAE ($F(1,28) = 19.46$, $p < 0.05$). To analyze the effect of temporal frequency we fitted straight lines to the functions relating the after-effect to temporal frequency. The slopes of the same-motion-direction condition were significantly different from zero for both the SFAE ($F(1,13) = 47.68$, $p < 0.05$) and SAAE ($F(1,13) = 7.874$, $p < 0.05$), whereas the slopes for the opposite motion direction conditions were not significantly different from zero for either the SFAE ($F(1,13) = 3.315$, $p = 0.0917$) or SAAE ($F(1,13) = 2.488$, $p = 0.1387$).

Control experiment 1: Apparent shape-frequency/shape-amplitude

A possible reason for the increase in the size of the SFAE/SAAE with temporal frequency when the adaptor and test moved in the same direction is that the apparent shape-frequencies of the adapting contours shifted to shape-frequencies more optimal for the after-effects. If so, then one would predict that adapting to static contours whose apparent shape-frequencies/shape-amplitudes were matched to those of the moving contours should increase the size of the after-effects to that of the moving contours. To test this prediction, subjects performed two experiments. The first determined the apparent shape-frequency and apparent shape-amplitude of a slow (1 c/deg) and a fast (6 c/deg) moving contour. The second experiment measured SFAEs/SAAEs using static adaptors whose shape-frequencies/shape-amplitudes were set to the apparent shape-frequencies/shape-amplitudes of the 1 and 6 c/sec moving contours, as determined from the first experiment.

For the shape-frequency matching experiment, we used a pair of contours consisting of a moving test contour of fixed shape-frequency and a static comparison contour whose shape-frequency was adjusted from trial to trial. We used two temporal frequencies for the moving test contour, 1 and 6 c/sec, with shape-frequencies of either 0.25 or 0.75 c/deg. The shape-amplitude of both test and comparison was set to 0.43 deg. The duration of each stimulus presentation was 1 sec. In the shape-amplitude matching experiment, the shape-amplitude of the moving test contour was fixed to either 0.25 or 0.75 c/deg and an adjustable shape-amplitude comparison contour. The shape-frequency of both test and comparison was 0.43 c/deg. On each trial the subject decided whether the test or comparison contour had the higher shape-frequency/shape-amplitude, and the PSE was obtained using the same staircase procedure as used with the after-effects.

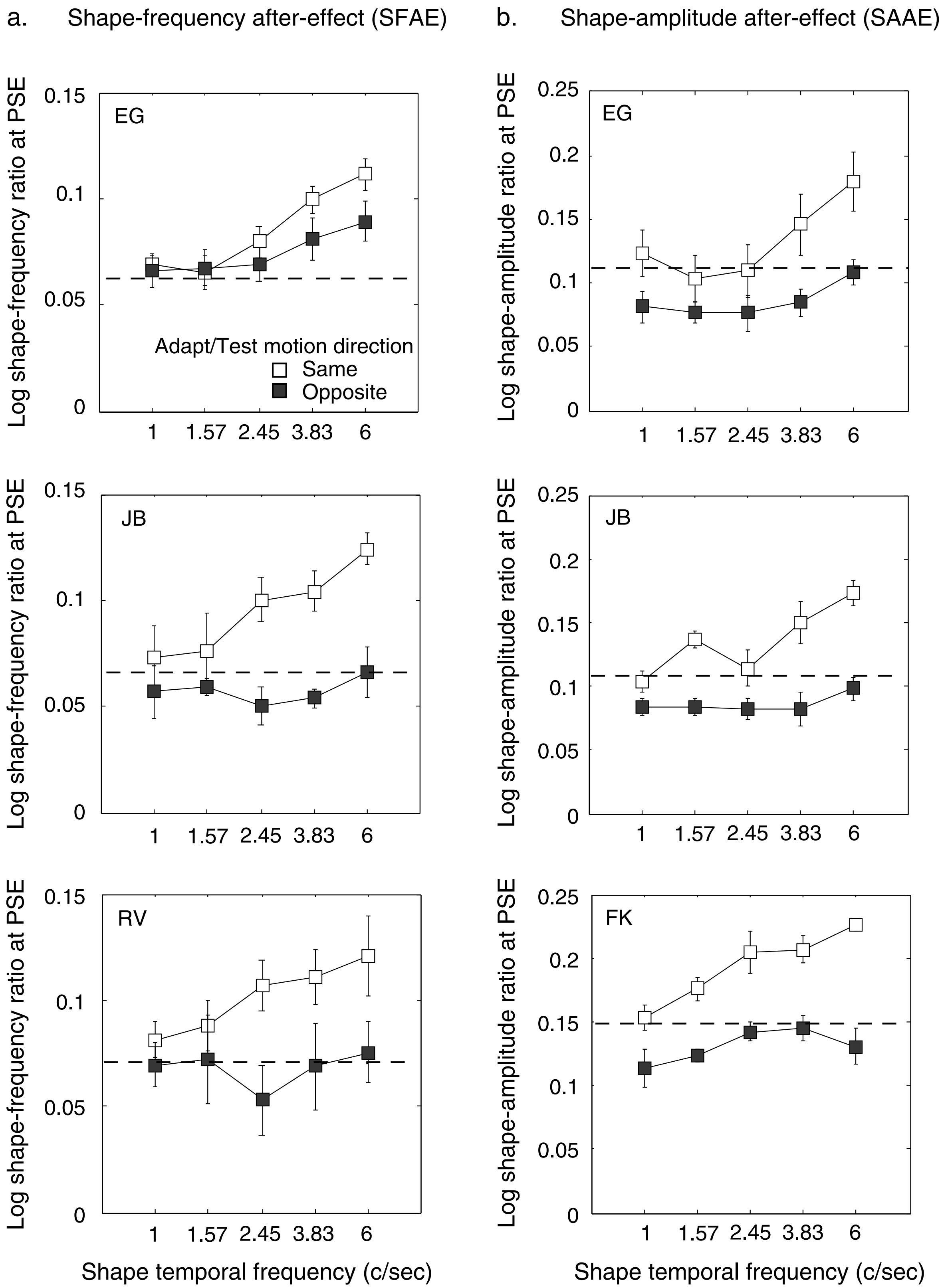

Figure 2. (a) SFAEs and (b) SAAEs as a function of temporal frequency for the same (open symbols) and opposite (filled symbols) adaptor-test motion direction conditions. The dashed lines indicate the size of after-effect obtained with static adaptor and test contours whose shape-phase changed randomly every 0.5 sec.

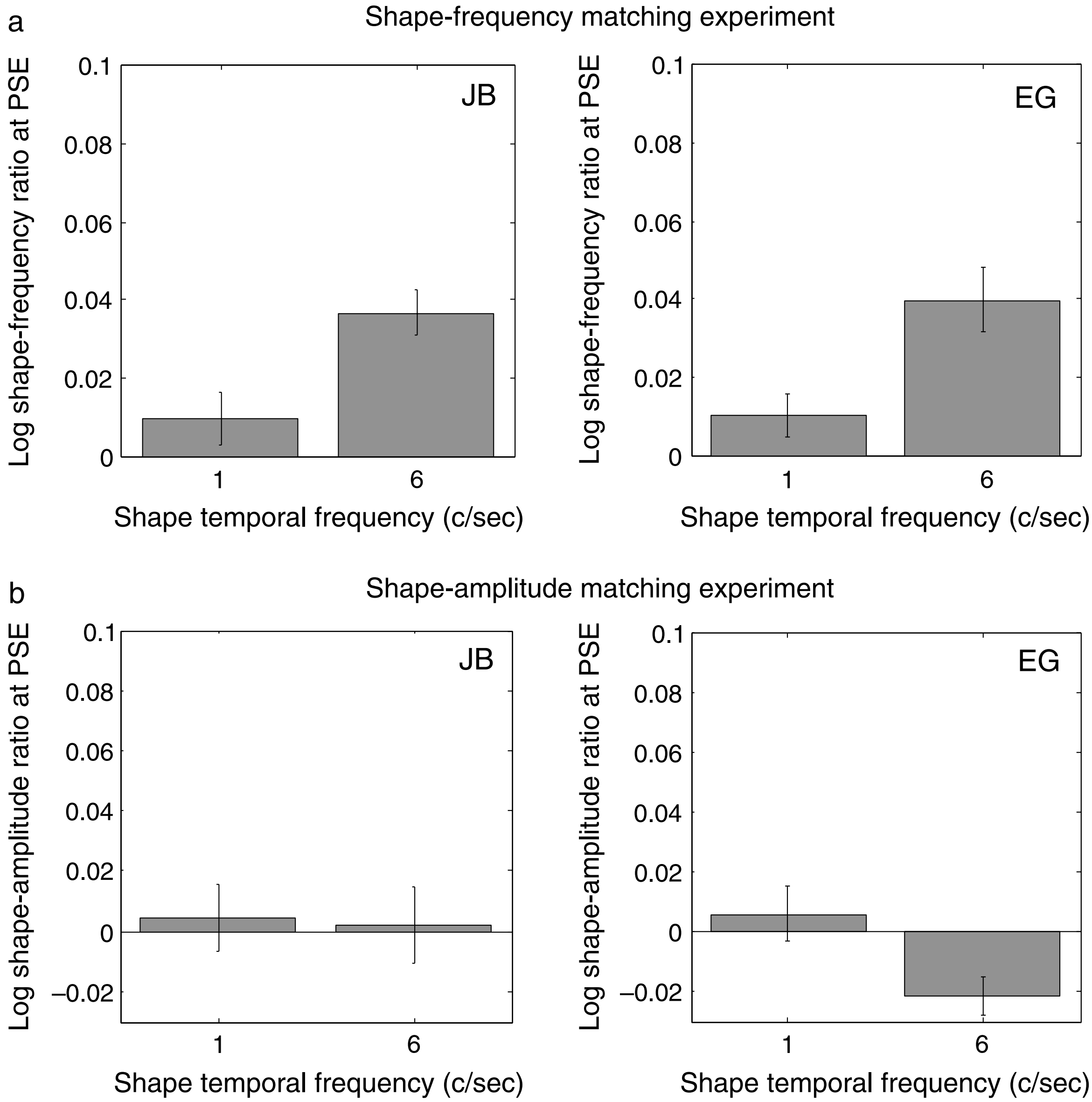

Figure 3. (a) Shape-frequency and (b) shape-amplitude matching results for temporal frequencies of 1 c/sec and 6 c/sec (see text for details).

The shape-frequency ratio at the PSE was calculated as the mean geometric ratio of the comparison (static) to test (moving) shape-frequencies/shape-amplitudes over the last 20 trials of the staircase. Two subjects (EG and JB) participated in this experiment.

Figure 3 shows the matching results for both temporal frequencies (1 and 6 c/sec) for shape-frequency (Figure 3a) and shape-amplitude (Figure 3b). The results demonstrate a significant increase in apparent shape-frequency when going from 1 c/sec to 6 c/sec but little, if any, change in apparent shape-amplitude. From the results we calculated that for the 1 c/sec temporal frequency, the apparent shape-frequencies of the 0.25 and 0.75 c/deg contours were respectively 0.263 and 0.747 c/deg for JB and 0.262 and 0.753 c/deg for EG. This represents on average an increase of ∼5% for the 0.25 c/deg and no increase for the 0.75 c/deg contours. For the 6 c/sec temporal frequency, the apparent shape-frequencies of the 0.25 and 0.75 c/deg contours were respectively 0.277 and 0.801 c/deg for subject JB and 0.287 and 0.79 c/deg for subject EG. This represents on average an increase in shape frequency of ∼13% for the 0.25 c/deg and ∼6% for the 0.75 c/deg contours from the static contour baseline.

The after-effects were then measured using static adaptors (as before with shape-phase randomized every 0.5 sec) set to the apparent shape-frequencies of the moving conditions (we only measured the SFAE as there were no significant changes in apparent shape-amplitude with motion). The test shape-frequency was set to the geometric mean shape-frequency of the two adaptors. Figure 4 shows SFAEs for static shape-frequencies matched to the 1 c/sec moving condition (the dark gray

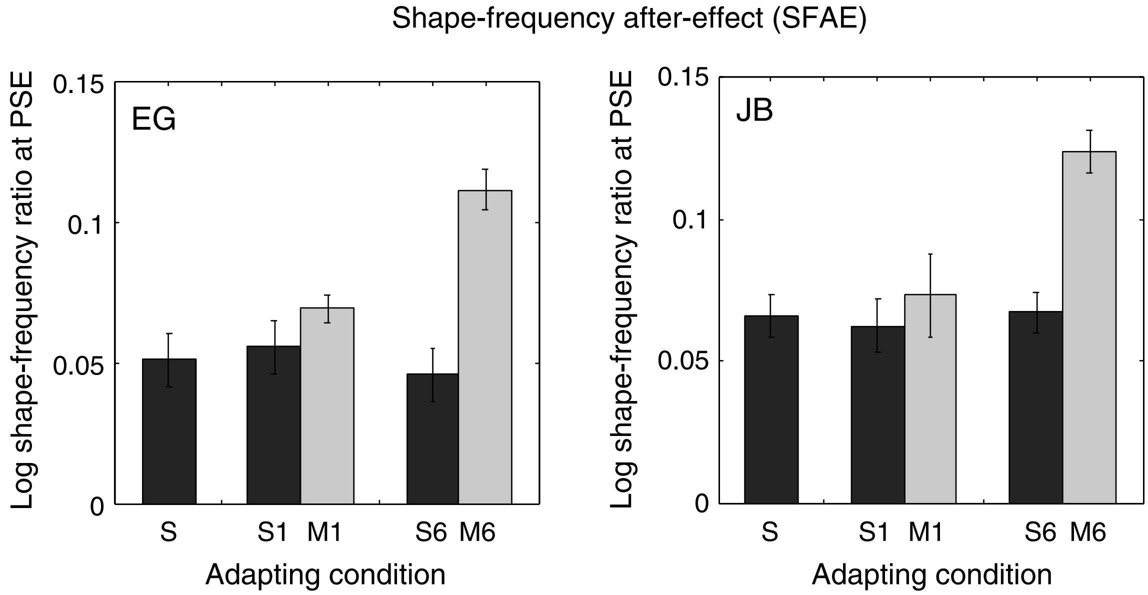

Figure 4. SFAEs for static adaptors with shape-frequencies of 0.25 and 0.75 c/deg (the dark gray bar labeled S), for static shape-frequencies matched to the 1 c/sec moving condition (the dark gray bar labeled S1) and to the 6 c/sec moving condition (the black bar labeled S6). For comparison reason we show SFAEs for 1 and 6 c/sec moving contour conditions (the light gray bars labeled M1 and M6, respectively).

bar labeled S1) and to the 6 c/sec moving condition (the black bar labeled S6). For comparison, we also show the SFAEs for the previously measured static condition with 0.25 and 0.75 c/deg adaptors (the dark gray bar labeled S) and for the previously measured 1 and 6 c/sec moving conditions (the light gray bars labeled M1 and M6, respectively). Figure 4 shows that all static conditions give similar sized SFAEs irrespective of the shape-frequencies of the adaptors/tests, with no hint of any static SFAE approaching the level of the 6 c/sec moving contour condition. This rules out the possibility that the increase in size of the SFAE with temporal frequency is a result of changes in apparent shape-frequency.

Control experiment 2: Motion-direction selectivity of the tilt after-effect?

A possible reason for the motion-direction selectivity of SFAE/SAAE found in Experiment 1 is that the after-effects are manifestations of the tilt after-effect (TAE), and that it is the TAE that is motion-direction selective. Carney (1982b) has reported motion direction selectivity for the TAE for gratings with spatial frequency of 1.64 c/deg and velocity 2.4 deg/sec. Although we have previously reported evidence suggesting that neither the SFAE nor SAAE are mediated by the TAE (Gheorghiu & Kingdom, 2007b) the experiments were carried out with static contours (with shape-phase randomized every 0.5 sec) and hence it is prudent to test for the involvement of the TAE with our moving contours. To do this we have used straight-line grating adaptors and sinusoidal-shaped contour tests, as illustrated in Figure 5a. If the motion-direction tuning of the TAE contributes to the motion-direction selectivity of the SFAE/SAAE, then drifting line-grating adaptors should produce motion-direction-selective shape after-effects in sine-wave-shaped contour tests.

We therefore compared after-effects for same and opposite directions using line-grating adaptors and sine-wave-shaped contour tests. We used two shape temporal frequencies: 1 and 6 cycles/sec. The line-grating adaptors had the same cross-sectional luminance profile as the sine-wave-shaped tests, and were spaced at the geometric mean periodicity of the tests. The line orientations were chosen on the basis of a Fourier analysis of the sinusoidal-shaped contours. This showed that the dominant orientations were at about ±32 deg from vertical for the previously used 0.75 c/deg contours and about ±62 deg from vertical for the previously used 0.25 c/deg contours (orientations very close to the tangents of the shape modulation at their d.c.), and so we used these orientations. During the adaptation period the grating orientation alternated between ± orientations (i.e. right and left) every 3 s in order to adapt both positive and negative orientations equally. We choose to alternate the orientations rather than present them together as a plaid in order to avoid the formation of angles at the intersection of the lines, which would clearly be capable of stimulating curvature mechanisms. Example adaptor and test are illustrated in Figure 5a and a movie is shown in Appendix A. In addition, we measured after-effects for static line gratings adaptor and test contours whose shape-phase changed randomly every 0.5 sec (the static condition). Two subjects (EG and JB) participated in this experiment.

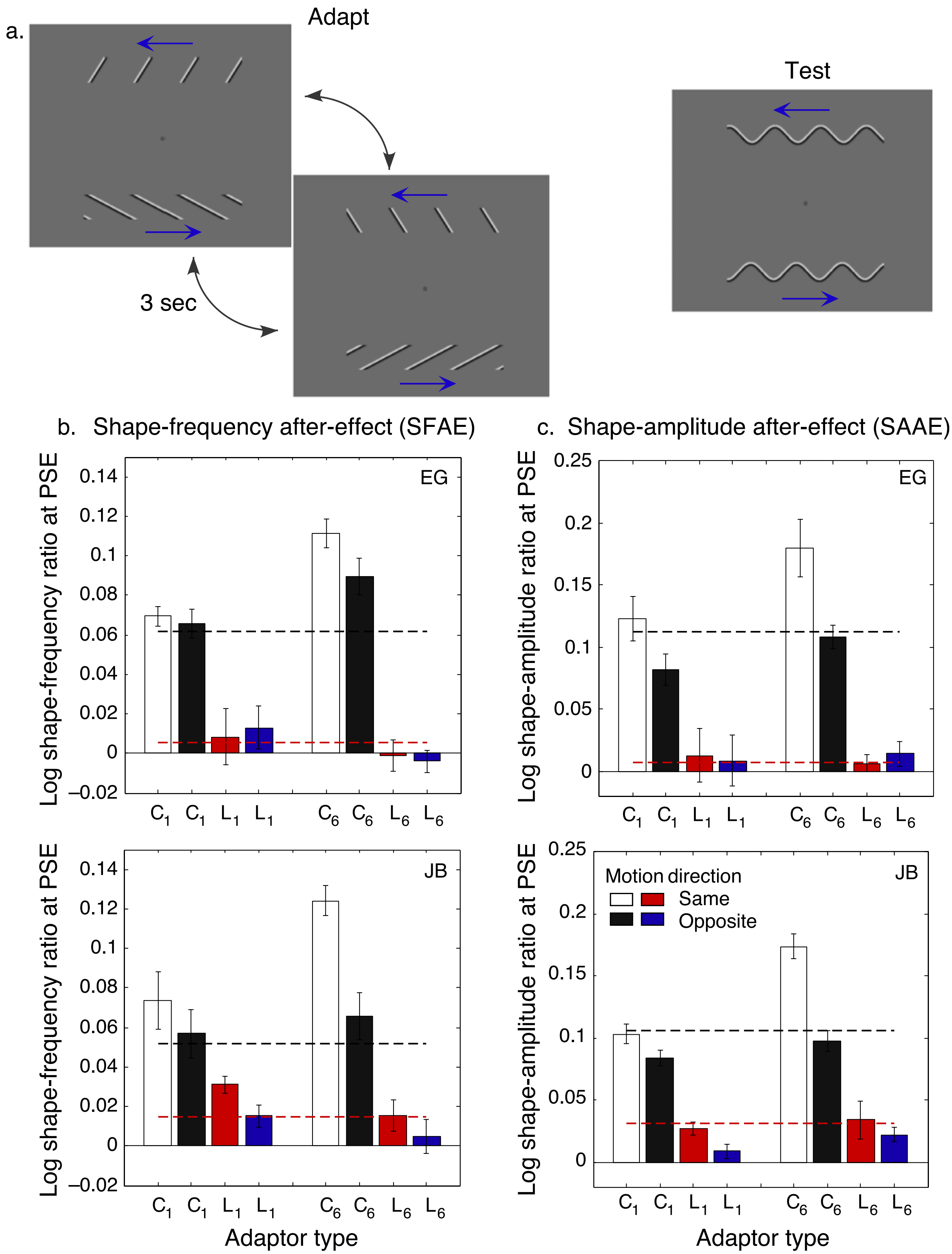

Figure 5. (a) Example line grating adaptor of alternating orientation moving in the same direction as the sinusoidal-shaped contour test; (b) SFAEs and (c) SAAEs for a line grating adaptor and contour test moving in the same (red) and opposite (blue) directions at shape temporal frequencies of 1 c/sec (the bars labeled L1) and 6 c/sec (the bars L6). For comparison we show SFAEs and SAAEs for a contour adaptor and a contour test moving in the same (white) and opposite (black) directions at 1 and 6 c/sec (the bars labeled C1 and C6, respectively). The dashed lines indicate the size of the after-effects obtained with a static line grating adaptor (red), a static contour adaptor (black) and a test contour whose shape-phase changed randomly every 0.5 sec.

Figure 5b shows SFAEs and Figure 5c SAAEs for the same (red bars) and opposite (blue bars) line-adaptor/sine-wave-shaped-test motion direction conditions, for 1 and 6 c/sec shape temporal frequency (the bars labeled L1 and L6, respectively). For comparison, we also show the previously measured SFAEs/SAAEs obtained with sine-wave-shaped adaptors and tests, for same (open bars) and opposite (black bars) motion directions, and for 1 and 6 c/sec (the bars labeled C1 and C6, respectively). The dashed lines indicate the size of the after-effects using static line-grating (red) and static sine-wave-shaped (black) adaptors/tests whose shape-phase changed randomly every 0.5 sec.

Figure 5 shows (i) prominently reduced SFAEs/SAAEs with line-grating adaptors compared to sine-wave-shaped adaptors (compare white-dark bars with red-blue bars); (ii) no differences between same and opposite motion directions with line-gratings adaptors and sine-wave-shaped tests (compare red and blue bars). These results make it extremely unlikely that the motion-direction selectivity of TAE is the reason for the motion-direction selectivity in the SFAE and SAAE.

Experiment 2: Effect of luminance spatial frequency

In this experiment we examine whether the pronounced global-motion-direction selectivity of the SFAE and SAAE found at high shape temporal frequencies (Experiment 1) is affected by the luminance spatial frequency of the moving contours.

Adaptor and test contours were constructed with odd-symmetric luminance profiles with various space-constants σ. Example contours are shown in Figure 1c. There were four σs: 0.122, 0.088, 0.044 and 0.022 deg. The peak luminance spatial frequency of the 1D-Gaussian luminance profile contours employed here is given by $1/2\pi\sigma$, resulting in luminance spatial frequencies of, respectively, 1.2, 1.81, 3.62 and 7.2 c/deg. We used adaptor-test contours moving either in the same or in opposite directions at 6 c/sec shape temporal frequency. The temporal frequency of 6 c/sec was employed as this produced the largest shape after-effects in the same motion-direction condition. In addition, we measured after-effects as a function of luminance spatial frequency for static adaptor and test contours whose shape-phase changed randomly every 0.5 sec (the static condition).

Figure 6 shows SFAEs (Figure 6a) and SAAEs (Figure 6b) as a function of luminance spatial frequency for the same (white symbols) and opposite (dark gray symbols) adaptor-test motion direction conditions. The static (light gray symbols) condition is also shown. The results show that SFAEs and SAAEs: (i) increase in magnitude with luminance spatial frequency in the same motion-direction condition, (ii) are lower and show no increase with luminance spatial frequency for the opposite motion direction conditions, and (iii) are lower and do not increase with luminance spatial frequency in the static condition. These results show that for a given shape temporal frequency, SFAEs and SAAEs are sensitive to luminance spatial frequency.

We ran a one-factor within-subjects ANOVA for the factor Motion-direction (same vs. opposite) and found a significant difference between the same and opposite conditions for both the SFAE ($F(1,2) = 7.26$, $p < 0.05$) and SAAE ($F(1,2) = 6.86$, $p < 0.05$). To analyze the effect of luminance spatial frequency we fitted straight lines to the functions relating the after-effect to luminance spatial frequency. The slopes of the same-motion-direction condition were significantly different from zero for both the SFAE ($F(1,10) = 5.010$, $p < 0.05$) and SAAE ($F(1,10) = 5.2$, $p < 0.05$), whereas the slopes for the opposite motion direction conditions were not significantly different from zero for either the SFAE ($F(1,10) = 0.039$, $p = 0.847$) or SAAE ($F(1,10) = 0.0001$, $p = 0.99$), as well as the slopes for the static condition for either the SFAE ($F(1,10) = 0.181$, $p = 0.678$) or SAAE ($F(1,10) = 0.003$, $p = 0.951$).

Why the positive impact of luminance spatial frequency on the size of both after-effects? One possibility is that it is because the size of the after-effect is proportional to luminance *temporal* frequency. Luminance temporal frequency is proportional to the product of luminance spatial frequency and shape temporal frequency, and hence for a given shape temporal frequency will be proportional to luminance spatial frequency. We tested the idea that luminance temporal frequency is the critical factor in the next experiment.

Experiment 3: Effect of luminance temporal frequency

Here we examine whether *luminance temporal frequency* is the critical factor behind the increase in after-effect magnitude with both shape temporal frequency and luminance spatial frequency. We measured after-effects for adaptors and tests moving in the same direction as a function of luminance spatial frequency for a low shape temporal frequency of 3 c/sec, and compared these results with those obtained in Experiment 2 from the relatively high shape temporal frequency 6 c/sec condition (open symbols in Figure 6). We used the same four values of luminance spatial frequency as in Experiment 2. This resulted in eight values of luminance temporal frequency: 8.75, 13.2, 17.5, 26.4, 52.5, and 105 c/sec. Two of these values (26.4 and 52.5 c/sec) were thus tested twice because they represented different combinations of luminance spatial frequency and shape temporal frequency. If luminance temporal frequency is the critical factor we would predict that the magnitude of the after-effects with

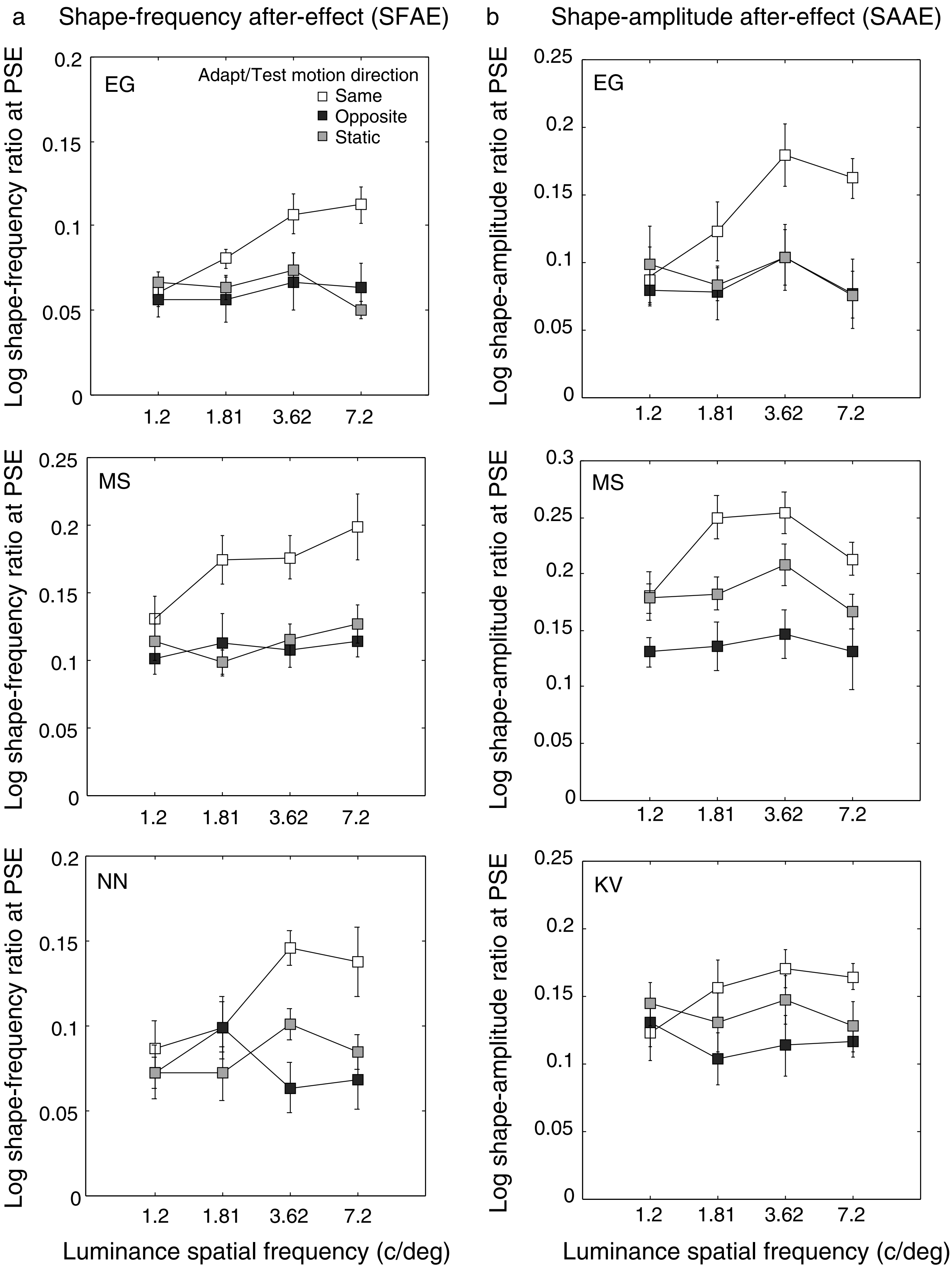

Figure 6. (a) SFAEs and (b) SAAEs as a function of luminance spatial frequency for the same (white symbols) and opposite (dark gray symbols) adaptor-test motion direction conditions, and static (light gray symbols) adaptor-test contours whose shape-phase changed randomly every 0.5 sec.

the 3 c/sec and 6 c/sec shape temporal frequencies would fall on a common line when plotted as a function of luminance temporal frequency.

Figure 7 shows the SFAEs (Figure 7a) and SAAEs (Figure 7b) for the same adaptor-test motion direction conditions as a function of luminance *spatial* frequency for 3 c/sec (filled symbols) and 6 c/sec (open symbols) shape temporal frequencies. The after-effects are reduced for the lower shape temporal frequency. Figure 8 shows the same data plotted as a function of luminance *temporal* frequency on a logarithmic scale. Figure 8 indicates that the two sets of data are brought closer together when plotted this way, but do not superimpose; they separate at high luminance temporal frequencies. These results suggest that luminance temporal frequency accounts for some, but not all of the variability in the size of the after-effects between different shape temporal frequencies. These data thus indicate that luminance temporal frequency *and* shape temporal frequency are factors determining the size of the SFAE and SAAE.

We ran a one-way ANOVA for the factor Shape temporal frequency (3 c/sec vs. 6 c/sec) and found a significant difference between the two shape temporal frequency conditions for both the SFAE ($F(1,22) = 22.82$, $p < 0.05$) and SAAE ($F(1,22) = 9.15$, $p < 0.05$). To analyze the effect of luminance spatial frequency we fitted straight lines to the functions relating the after-effect to luminance spatial frequency for the 3 c/sec and 6 c/sec shape temporal frequency. For both shape temporal frequencies, the slopes of the same-motion-direction condition were significantly different from zero for both the SFAE ($F(1,10) = 13.45$, $p < 0.05$ for 3 c/sec and $F(1,10) = 5.010$, $p < 0.05$ for 6 c/sec) and SAAE ($F(1,10) = 5.235$, $p < 0.05$ for 3 c/sec and $F(1,10) = 5.2$, $p < 0.05$ for 6 c/sec).

Experiment 4: Local motion-direction tuning

In this experiment we investigate whether curvature-encoding mechanisms are selective for *local* motion direction. To do this we compared the magnitude of the shape after-effects for same with opposite local-motion-direction adaptors and tests.

To examine local motion direction selectivity, we used adaptor/test contours constructed from Gabor patches with a spatial bandwidth of 1.5 octaves and spatial frequency of 3.62 c/deg (see Figure 1d). The spacing between the Gabor patches along the contour was 0.4 deg. Gabor contrast was set to 0.85. Because the Gabor-string contours were contained within a fixed width stimulus window, the number of Gabor patches differed by a factor of 1.28 between the two adaptors: the high shape-frequency or shape amplitude contours had 27 Gabors, the low shape-frequency or shape amplitude adaptors had 21 Gabors. The orientation of each Gabor patch was tangential to the shape of the contour, in order to make them as collinear as possible. The envelopes of the Gabor patches were stationary while the carriers moved with different velocities such that their motions simulated that of a rigid-body contour-shape (see black arrows in Figure 1d). To do this, the velocity of each carrier was defined as the product of the luminance temporal frequency of the carrier and the cosine of the Gabor's orientation (with respect to vertical). As a result the *perceived* global motion direction for the Gabor-string was either leftward (see blue arrows in Figure 1d) or rightward. Example contours are shown in Figure 1d and a movie is provided in Appendix A. As elsewhere we compared same adaptor-test with opposite adaptor-test motion directions on both the SFAE and SAAE.

The adaptor pair for the SFAE consisted of contours with a shape-amplitude of 0.35 deg and shape frequencies of 0.2 and 0.6 c/deg, giving a geometric mean shape-frequency of 0.35 c/deg. For the SAAE, the adaptor pair consisted of contours with a shape-frequency of 0.35 c/deg and shape amplitudes of 0.2 and 0.6 deg, giving a geometric mean shape-amplitude of 0.35 deg. During the adaptation period the contour's shape-phase changed randomly every 3 sec. We had intended to use three values of the horizontal component of luminance temporal frequency, i.e. that of the rigid-body contour shape: 8.4, 20.6 and 50.2 c/sec. These corresponded to the shape temporal frequencies of 1, 2.45 and 6 c/sec used in Experiment 1. We found however that at 50.2 c/sec observers perceived only flicker and no directional motion, so we did not test this condition. In addition, we measured the after-effects with adaptor and test contours consisting of Gabor patches with static carriers, while changing the contour's shape-phase randomly every 3 sec. This was the static condition.

Figure 9 shows SFAEs (Figure 9a) and SAAEs (Figure 9b) for same (open symbols) and opposite (filled symbols) adaptor-test local motion directions, as a function of carrier luminance temporal frequency. The dashed lines indicate the magnitude of the after-effects obtained with static Gabors. It is clear from the figure that SFAEs/SAAEs are similar for same and opposite motion directions (compare open and filled symbols) and for slow (8.4 c/sec) and relatively fast (20.6 c/sec) luminance temporal frequencies.

We ran a one-factor ANOVA for the factor Motion direction (same vs. opposite) and found that Motion direction is not significantly different for both the SFAE ($F(1,10) = 1.85$, $p > 0.05$) and SAAE ($F(1,10) = 0.08$, $p > 0.05$). We confirmed the lack of effect of temporal frequency by fitting straight lines to the functions relating the after-effects to luminance temporal frequency, and found that none of them was significantly different from zero. The slopes of the same-motion-direction condition were not significantly different from zero for both the SFAE ($F(1,4) = 1.266$, $p > 0.05$) and SAAE ($F(1,4) =$

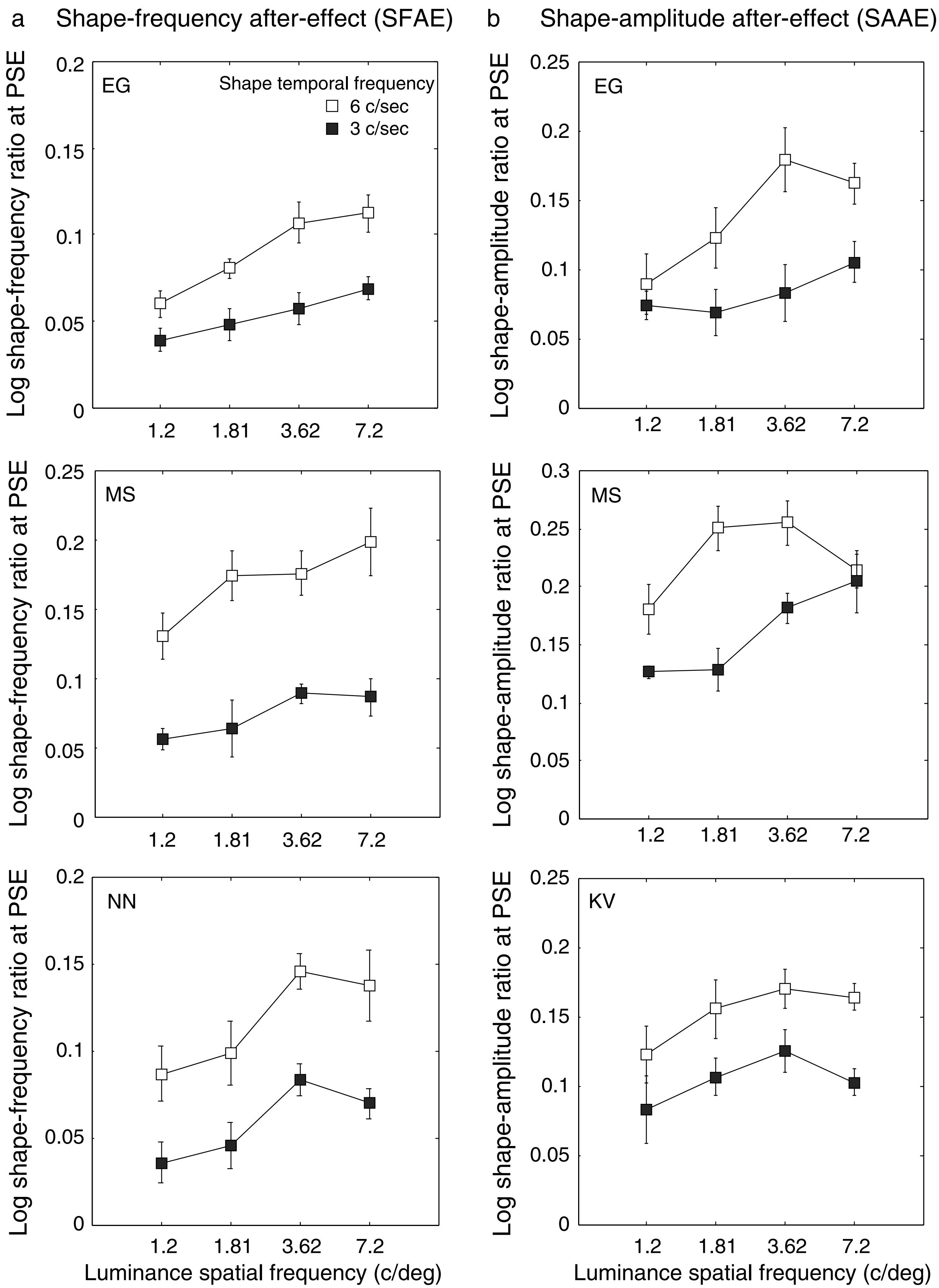

Figure 7. (a) SFAEs and (b) SAAEs for same adaptor-test motion-direction condition as a function of luminance spatial frequency for 3 c/sec (filled symbols) and 6 c/sec (open symbols) shape temporal frequencies.

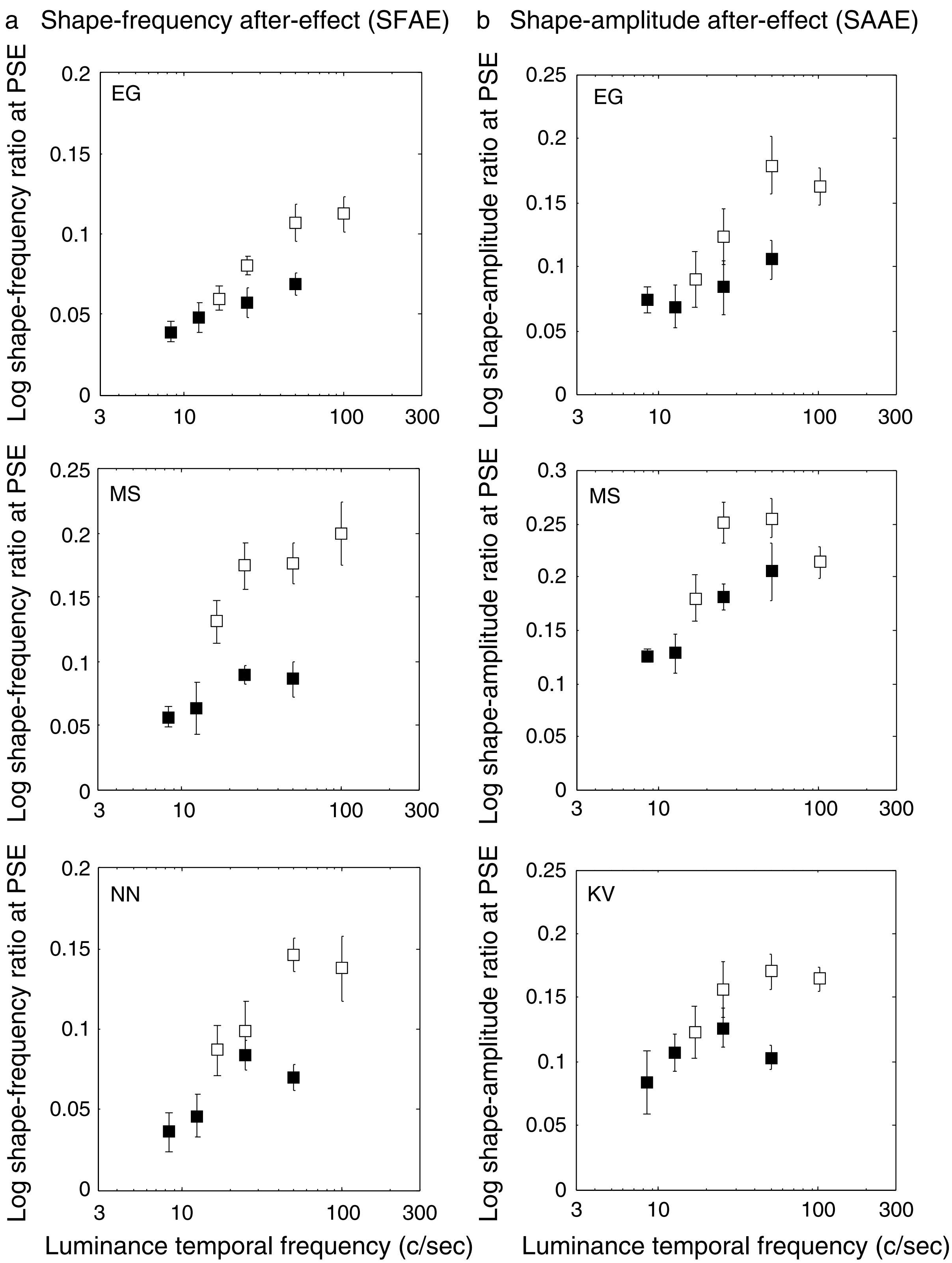

Figure 8. (a) SFAEs and (b) SAAEs for same adaptor-test motion-direction condition as a function of luminance temporal frequency plotted on a logarithmic axis.

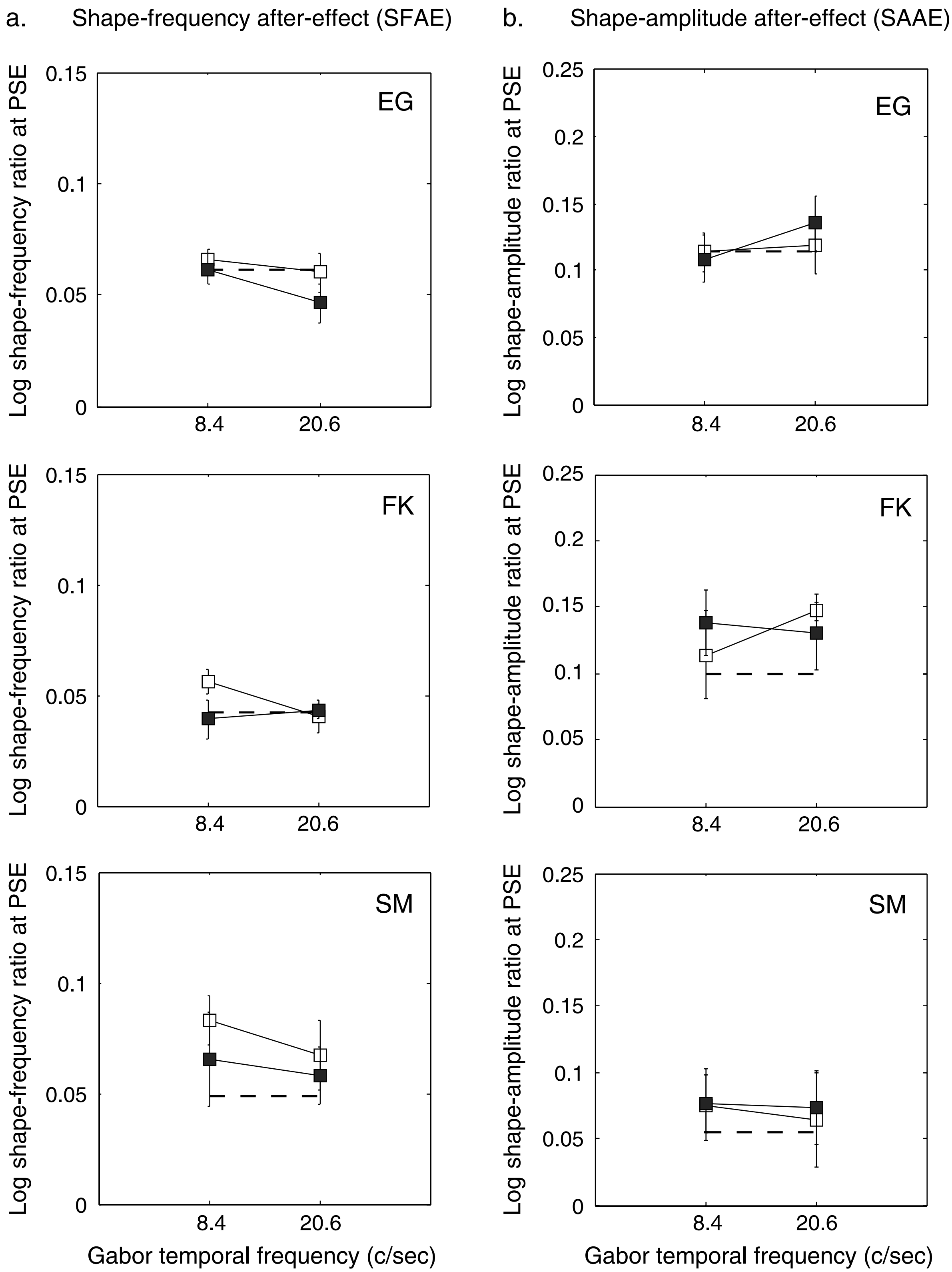

Figure 9. (a) SFAEs and (b) SAAEs as a function of luminance temporal frequency for the same (open symbols) and opposite (filled symbols) adaptor-test local-motion-direction conditions. The dashed lines indicate the size of after-effect obtained with static adaptor and test contours whose shape-phase changed randomly every 3 sec.

1.1104, $p > 0.05$), and for the opposite motion direction conditions for the SFAE ($F(1,4) = 0.422$, $p > 0.05$) and SAAE ($F(1,4) = 0.0396$, $p > 0.05$).

General discussion

Using two curvature after-effects—the SFAE and SAAE—we investigated the selectivity of curvature-sensitive mechanisms to global (i.e. whole contour) motion direction, as well as sensitivity to shape temporal frequency, luminance spatial frequency and luminance temporal frequency. We also examined local (carrier-only) motion direction selectivity. We found that both SFAEs and SAAEs showed selectivity to global motion direction but neither after-effect showed selectivity for local motion direction. With global motion, we found that provided the adaptor and test moved in the same direction, the after-effects increased in magnitude with (i) shape temporal frequency and (ii) luminance spatial frequency. A control experiment ruled out that the increase in the SFAE/SAAE with shape temporal frequency was caused by changes in the *apparent* shape-frequencies/shape-amplitudes of the contours with shape temporal frequency. An additional control experiment ruled out that the motion-direction selectivity was due to the tilt after-effect (TAE). Finally, while the dependency on shape-temporal and luminance-spatial frequency was shown to be partly explained by luminance temporal frequency, shape temporal frequency also appeared to play a role.

The sensitivity to luminance spatial and luminance temporal frequency in the global motion condition is perhaps not surprising given the wealth of evidence that low-level motion mechanisms are sensitive to these properties (Albrecht & Geisler, 1991; Anderson & Burr, 1985, 1989; O'Keefe & Movshon, 1998; Pantle, Lehmkuhle, & Caudill, 1978). Why however is there a positive influence of shape temporal frequency over and above that of its effect on luminance temporal frequency, at least in the same-direction global-motion condition? One is tempted to think that direction-selective curvature detectors are tuned to relatively high temporal frequencies. The problem with this explanation is that on its own it fails to account for the absence of any effect of luminance temporal frequency in the local motion condition. Another possibility is that if the temporal integration window for stimulating a curvature detector is relatively short, more curvature detectors lying within the stimulus window will be stimulated by a medium-to-high shape temporal frequency than to a low one. In other words, the fast-moving whole contours provide more effective spatio-temporal coverage. If the coverage explanation is correct, then this study serves as a salutary lesson in showing that the local motion paradigm might not always be the best method of revealing the motion properties of contour-sensitive mechanisms.

How do our results compare with those of other after-effects? A number of studies have revealed motion direction selectivity for various spatial after-effects such as the tilt after-effect (Apthorp & Alais, 2009; Carney, 1982a, 1982b) and the size after-effect (Nishida et al., 1999). Carney (1982a, 1982b) obtained motion direction selectivity for the tilt after-effect at a spatial frequency of 1.64 c/deg and velocity of 2.4 deg/sec. Nishida et al. (1999) showed weak but significant direction selectivity for the size after-effect only for low spatial and high temporal frequencies (0.5 cpd/8 Hz) in support of the idea that there are at least some neurons that are involved in processing spatial frequency that are also direction-selective. Could the coverage explanation account for the non-selectivity to motion-direction of the size after-effect at low temporal frequencies in the Nishida et al.'s (1999) study? The drifting gratings used by Nishida et al. completely filled the stimulus window, so it is hard to see how the coverage explanation would in this case apply.

Relationship to neurophysiology

In the neurophysiological literature, direction-selectivity in shape-processing has been studied mainly with the aim of establishing whether neurons in areas such as V4 and IT are cue-invariant, that is selective for shape irrespective of whether defined by luminance contrast, relative motion, disparity or texture (Mysore et al., 2006; Sary et al., 1995; Sary et al., 1993; Tanaka, Uka, Yoshiyama, Kato, & Fujita, 2001; Vogels & Orban, 1996). For example Mysore et al. (2006) found V4 neurons that had similar preferences for shapes defined either by relative motion or luminance contrast. The neurons however were not selective to the direction of the motion-defined shapes, might seem to contradict the results of the present study. However one should not necessarily expect that motion-defined shapes have the same psychophysical properties as moving luminance-defined shapes. If the main purpose of detecting motion-defined shapes is figure-ground segregation, this might be a sufficient end in itself, with no need for the visual system to label the encoded shapes for their motion direction.

Neurophysiological studies have shown that neurons in area V4 of macaques do not show selectivity for direction of motion, as measured from their responses to directional stimuli (Desimone & Schein, 1987). However, recent studies have shown that classically non-directional V4 neurons develop motion direction selectivity after motion adaptation, a finding that emphasizes the dynamic nature of functional cortical architecture (Tolias, Keliris, Smirnakis, & Logothetis, 2005). In a functional magnetic resonance imaging (fMRI) study, Tolias, Smirnakis, Augath, Trinath, and Logothetis (2001) used a motion adaptation paradigm to study properties of populations of neurons in macaque

V4. They found a high direction-of-motion selectivity index, suggesting that the adaptation-dependent selectivity might arise from feedback from higher visual areas.

Appendix A

Example contours undergoing global and local motion.

Movie A.

A

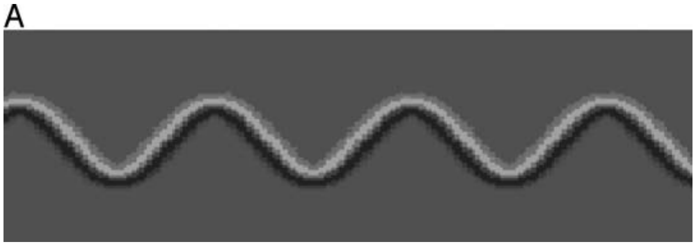

Movie A. Global motion-direction.

Movie B.

B

Movie B. Local motion-direction.

Movie C.

C

Movie C. Example line gratings adaptor and sinusoidal-shaped contour.

Acknowledgments

This research was supported by a Natural Sciences and Engineering Research Council of Canada (NSERC) grant # OGP01217130 given to F.K. and by a Research Foundation—Flanders (Fonds Wetenschappelijk Onderzoek—Vlaanderen) fellowship given to E.G.

Commercial relationships: none.

Corresponding author: Elena Gheorghiu.
Email: elena.gheorghiu@psy.kuleuven.be.
Address: Laboratory of Experimental Psychology, University of Leuven, Tiensestraat 102, B-3000 Leuven, Belgium.

References

Albrecht, D. G., & Geisler, W. S. (1991). Motion selectivity and the contrast-response function of simple cells in the visual cortex. *Visual Neuroscience, 7,* 531–546. [PubMed]

Anderson, N. D., Habak, C., Wilkinson, F., & Wilson, H. R. (2007). Evaluating shape after-effects with radial frequency patterns. *Vision Research, 47,* 298–308. [PubMed]

Anderson, S. J., & Burr, D. C. (1985). Spatial and temporal selectivity of the human motion detection system. *Vision Research, 25,* 1147–1154.

Anderson, S. J., & Burr, D. C. (1989). Receptive field properties of human motion detector units inferred from spatial frequency masking. *Vision Research, 29,* 1343–1358. [PubMed]

Apthorp, D., & Alais, D. (2009). Tilt aftereffects and tilt illusions induced by fast translational motion: Evidence for motion streaks. *Journal of Vision, 9*(1):27, 1–11, http://journalofvision.org/9/1/27/, doi:10.1167/9.1.27. [PubMed] [Article]

Baizer, J. S., Ungerleider, L. G., & Desimone, R. (1991). Organization of visual inputs to the inferior temporal and posterior parietal cortex in macaques. *Journal of Neuroscience, 11,* 168–190. [PubMed] [Article]

Bell, J., & Kingdom, F. A. (2009). Global contour shapes are coded differently from their local components. *Vision Research, 49,* 1702–1710.

Bex, P. J., Simmers, A. J., & Dakin, S. C. (2003). Grouping local directional signals into moving contours. *Vision Research, 43,* 2141–2153. [PubMed]

Carney, T. (1982a). Direction-specific tilt illusion: With and without gaze fixation. *Perception, 11,* 529–533. [PubMed]

Carney, T. (1982b). Directional specificity in tilt aftereffect induced with moving contours: A reexamination. *Vision Research, 22,* 1273–1275. [PubMed]

Connor, C. E., Brincat, S. L., & Pasupathy, A. (2007). Transformation of shape information in the ventral pathway. *Current Opinion Neurobiology, 17,* 140–147. [PubMed]

De Valois, R. L., & De Valois, K. K. (1991). Vernier acuity with stationary moving Gabors. *Vision Research, 31,* 1619–1626. [PubMed]

Desimone, R., & Schein, S. J. (1987). Visual properties of neurons in area V4 of the macaque: Sensitivity to stimulus form. *Journal of Neurophysiology, 57,* 835–868. [PubMed]

Gallant, J. L., Braun, J., & Van Essen, D. C. (1993). Selectivity for polar, hyperbolic, and Cartesian gratings in Macaque visual cortex. *Science, 259,* 100–103. [PubMed]

Gallant, J. L., Connor, C. E., Rakshit, S., Lewis, J. W., & Van Essen, D. C. (1996). Neural responses to polar, hyperbolic, and Cartesian gratings in area V4 of the Macaque monkey. *Journal of Neurophysiology, 76,* 2718–2739. [PubMed]

Gheorghiu, E., & Kingdom, F. A. (2006). Luminance-contrast properties of contour-shape processing revealed through the shape-frequency after-effect. *Vision Research, 46,* 3603–3615. [PubMed]

Gheorghiu, E., & Kingdom, F. A. (2007a). Chromatic tuning of contour-shape mechanisms revealed through the shape-frequency and shape-amplitude after-effects. *Vision Research, 47,* 1935–1949. [PubMed]

Gheorghiu, E., & Kingdom, F. A. (2007b). The spatial feature underlying the shape-frequency and shape-amplitude after-effects. *Vision Research, 47,* 834–844. [PubMed]

Gheorghiu, E., & Kingdom, F. A. (2008). Spatial properties of curvature-encoding mechanisms revealed through the shape-frequency and shape-amplitude after-effects. *Vision Research, 48,* 1107–1124. [PubMed]

Gheorghiu, E., & Kingdom, F. A. (2009). Multiplication in curvature processing. *Journal of Vision, 9*(2):23, 1–17, http://journalofvision.org/9/2/23/, doi:10.1167/9.2.23. [PubMed] [Article]

Gheorghiu, E., Kingdom, F. A., Thai, M. T., & Sampasivam, L. (2009). Binocular properties of curvature-encoding mechanisms revealed through two shape after-effects. *Vision Research, 49,* 1765–1774. [PubMed]

Habak, C., Wilkinson, F., Zakher, B., & Wilson, H. R. (2004). Curvature population coding for complex shapes in human vision. *Vision Research, 44,* 2815–2823. [PubMed]

Hayes, A. (2000). Apparent position governs contour-element binding by the visual system. *Proceedings of the Royal Society London B: Biological Sciences, 267,* 1341–1345. [PubMed] [Article]

Hess, R. F., & Ledgeway, T. (2003). The detection of direction-defined and speed-defined spatial contours: One mechanism or two? *Vision Research, 43,* 597–606. [PubMed]

Ito, M., Tamura, H., Fujita, I., & Tanaka, K. (1995). Size and position invariance of neuronal responses in monkey inferotemporal cortex. *Journal of Neurophysiology, 73,* 218–226.

Ledgeway, T., & Hess, R. F. (2002). Rules for combining the outputs of local motion detectors to define simple contours. *Vision Research, 42,* 653–659. [PubMed]

Levi, D. M., & Klein, S. A. (2000). Seeing circles: What limits shape perception? *Vision Research, 40,* 2329–2339. [PubMed]

Loffler, G., & Wilson, H. R. (2001). Detecting shape deformation of moving patterns. *Vision Research, 41,* 991–1006. [PubMed]

Maunsell, J. H., & van Essen, D. C. (1983). The connections of the middle temporal visual area (MT) and their relationship to a cortical hierarchy in the macaque monkey. *Journal of Neuroscience, 3,* 2563–2586. [PubMed] [Article]

Merigan, W. H., & Maunsell, J. H. (1993). How parallel are the primate visual pathways? *Annual Reviews of Neuroscience, 16,* 369–402. [PubMed]

Missal, M., Vogels, R., Li, C. Y., & Orban, G. A. (1999). Shape interactions in macaque inferior temporal neurons. *Journal of Neurophysiology, 82,* 131–142. [PubMed] [Article]

Murray, S. O., Kersten, D., Olshausen, B. A., Schrater, P., & Woods, D. L. (2002). Shape perception reduces activity in human primary visual cortex. *Proceedings National Academy of Science of the United States of America, 99,* 15164–15169. [PubMed] [Article]

Mysore, S. G., Vogels, R., Raiguel, S. E., & Orban, G. A. (2006). Processing of kinetic boundaries in macaque V4. *Journal of Neurophysiology, 95,* 1864–1880. [PubMed] [Article]

Mysore, S. G., Vogels, R., Raiguel, S. E., & Orban, G. A. (2008). Shape selectivity for camouflage-breaking dynamic stimuli in dorsal V4 neurons. *Cerebral Cortex, 18,* 1429–1443.

Nishida, S., Motoyoshi, I., & Takeuchi, T. (1999). Is the size aftereffect direction selective? *Vision Research, 39,* 3592–3601. [PubMed]

O'Keefe, L. P., & Movshon, J. A. (1998). Processing of first- and second-order motion signals by neurons in area MT of the macaque monkey. *Visual Neuroscience, 15,* 305–317.

Pantle, A., Lehmkuhle, S., & Caudill, M. (1978). On the capacity of directionally selective mechanisms to encode different dimensions of moving stimuli. *Perception, 7,* 261–267.

Pasupathy, A., & Connor, C. E. (2001). Shape representation in area V4: Position specific tuning for boundary conformation. *Journal of Neurophysiology, 86,* 2505–2519. [PubMed] [Article]

Pasupathy, A., & Connor, C. E. (2002). Population coding of shape in area V4. *Nature Neuroscience, 5,* 1332–1338. [PubMed]

Prins, N., Kingdom, F. A. A., & Hayes, A. (2007). Detecting low shape-frequencies in smooth and jagged contours. *Vision Research, 47,* 2390–2402. [PubMed]

Rainville, S. J., & Wilson, H. R. (2004). The influence of motion-defined form on the perception of spatially-defined form. *Vision Research, 44,* 1065–1077. [PubMed]

Rainville, S. J., & Wilson, H. R. (2005). Global shape coding for motion-defined radial-frequency contours. *Vision Research, 45,* 3189–3201.

Regan, D., & Hamstra, S. J. (1992). Shape discrimination and the judgement of perfect symmetry: Dissociation of shape from size. *Vision Research, 32,* 1845–1864. [PubMed]

Sary, G., Vogels, R., Kovacs, G., & Orban, G. A. (1995). Responses of monkey inferior temporal neurons to luminance-, motion-, and texture-defined gratings. *Journal of Neurophysiology, 73,* 1341–1354. [PubMed]

Sary, G., Vogels, R., & Orban, G. A. (1993). Cue-invariant shape selectivity of macaque inferior temporal neurons. *Science, 260,* 995–997. [PubMed]

Shipp, S. (1995). Visual processing. The odd couple. *Current Biology, 5,* 116–119. [PubMed]

Tanaka, H., Uka, T., Yoshiyama, K., Kato, M., & Fujita, I. (2001). Processing of shape defined by disparity in monkey inferior temporal cortex. *Journal of Neurophysiology, 85,* 735–744. [PubMed] [Article]

Tanaka, K. (1996). Inferotemporal cortex and object vision. *Annual Review of Neuroscience, 19,* 109–139. [PubMed]

Thompson, P. (1981). Velocity after-effects: The effects of adaptation to moving stimuli on the perception of subsequently seen moving stimuli. *Vision Research, 21,* 337–345. [PubMed]

Tolias, A. S., Keliris, G. A., Smirnakis, S. M., & Logothetis, N. K. (2005). Neurons in macaque area V4 acquire directional tuning after adaptation to motion stimuli. *Nature Neuroscience, 8,* 591–593. [PubMed]

Tolias, A. S., Smirnakis, S. M., Augath, M. A., Trinath, T., & Logothetis, N. K. (2001). Motion processing in the macaque: Revisited with functional magnetic resonance imaging. *Journal of Neuroscience, 21,* 8594–8601. [PubMed] [Article]

Ungerleider, L. G., & Desimone, R. (1986). Cortical connections of visual area MT in the macaque. *Journal of Computer Neurology, 248,* 190–222. [PubMed]

Van Essen, D. C., Maunsell, J. H., & Bixby, J. L. (1981). The middle temporal visual area in the macaque: Myeloarchitecture, connections, functional properties and topographic organization. *Journal of Computerize Neurology, 199,* 293–326.

Vogels, R., & Orban, G. A. (1996). Coding of stimulus invariances by inferior temporal neurons. *Program Brain Research, 112,* 195–211. [PubMed]

Wang, J., Zhou, T., Qiu, M., Du, A., Cai, K., Wang, Z., et al. (1999). Relationship between ventral stream for object vision and dorsal stream for spatial vision: An fMRI + ERP study. *Human Brain Mapping, 8,* 170–181.

Wilkinson, F., Wilson, H. R., & Habak, C. (1998). Detection and recognition of radial frequency patterns. *Vision Research, 38,* 3555–3568. [PubMed]

Wilson, H. R., & Richards, W. A. (1989). Mechanisms of contour curvature discrimination. *Journal of Optical Society of America A, Optics and Image Science, 6,* 106–115. [PubMed]